HHS Public Access

Author manuscript

Acad Radiol. Author manuscript; available in PMC 2023 January 01.

Published in final edited form as:

Acad Radiol. 2022 January ; 29(Suppl 1): S223–S228. doi:10.1016/j.acra.2020.10.015.

Optimizing the peritumoral region size in radiomic analysis for sentinel lymph node status prediction in breast cancer

Jie Ding, PhD[1,2], **Shenglan Chen, MS**[1], **Mario Serrano Sosa, MS**[1], **Renee Cattell, PhD**[1], **Lan Lei, MS**[3], **Junqi Sun, MD**[4,5], **Prateek Prasanna, PhD**[6], **Chunling Liu, MD**[4,7], **Chuan Huang, PhD**[1,4,8,*]

[1]Department of Biomedical Engineering, Stony Brook University, 100 Nicolls Rd, Stony Brook, NY 11794, USA;

[2]Department of Radiation Oncology, Medical College of Wisconsin, 8701 W Watertown Plank Rd, Wauwatosa, WI 53226, USA;

[3]Pogram in Program in Public Health, Renaissance School of Medicine, Stony Brook University, 100 Nicolls Rd, Stony Brook, NY 11794, USA;

[4]Department of Radiology, Renaissance School of Medicine, Stony Brook University, 100 Nicolls Rd, Stony Brook, NY 11794, USA;

[5]Department of Radiology, Yuebei People's Hospital, 133 Huimin S Rd, Shaoguan, Guangdong 512025, China;

[6]Department of Biomedical Informatics, Renaissance School of Medicine, Stony Brook University, 100 Nicolls Rd, Stony Brook, NY 11794, USA;

[7]Department of Radiology, Guangdong General Hospital/Guangdong Academy of Medical Sciences, 106 Zhongshan 2nd Rd, Guangzhou, Guangdong 510080, China;

[8]Department of Psychiatry, Renaissance School of Medicine, Stony Brook University, 100 Nicolls Rd, Stony Brook, NY 11794, USA.

Abstract

Rationale and Objectives—Peritumoral features have been suggested to be useful in improving the prediction performance of radiomic models. The aim of this study is to systematically investigate the prediction performance improvement for sentinel lymph node (SLN) status in breast cancer from peritumoral features in radiomic analysis by exploring the effect of peritumoral region sizes.

Materials and Methods—This retrospective study was performed using DCE-MRI scans of 162 breast cancer patients. The effect of peritumoral features was evaluated in a radiomics pipeline for predicting SLN metastasis in breast cancer. Peritumoral regions were generated by dilating the tumor regions-of-interest (ROIs) manually annotated by two expert radiologists, with thicknesses of 2mm, 4mm, 6mm and 8mm. The prediction models were established in the training set (~67%

[*]**Corresponding author info:** Chuan Huang, PhD, Department of Radiology, HSC L4-120, Renaissance School of Medicine, Stony Brook University, 100 Nicolls Rd, Stony Brook, NY 11794, USA. Phone: 631-444-6905; Fax: 631-444-6450; chuan.huang@stonybrookmedicine.edu.

of cases) using the radiomics pipeline with and without peritumoral features derived from different peritumoral thicknesses. The prediction performance was tested in an independent validation set (the remaining ~33%).

Results—For this specific application, the accuracy in the validation set when using the two radiologists' ROIs could be both improved from 0.704 to 0.796 by incorporating peritumoral features. The choice of the peritumoral size could affect the level of improvement.

Conclusion—This study systematically investigates the effect of peritumoral region sizes in radiomic analysis for prediction performance improvement. The choice of the peritumoral size is dependent on the ROI drawing and would affect the final prediction performance of radiomic models, suggesting that peritumoral features should be optimized in future radiomics studies.

Keywords

Radiomics; peritumoral features; DCE-MRI; breast cancer; sentinel lymph node status

Introduction

Radiomics, a technique based on extracting high-dimensional quantitative image features to provide non-invasive biomarkers for clinical outcomes, has drawn marked interest in recent years(1–3). It has been shown to be a powerful tool which could support clinical decision making. Radiomic features are able to capture the heterogeneity and complexity of the tumor microenvironment(2). Whereas radiomic features are mostly impossible for humans to perceive, they can be predictive of the tumor status and easily used to develop models pertaining to clinical outcomes.

As MRI becomes increasingly common for breast cancer in clinical practice, recent studies have demonstrated that MRI-based radiomics can predict recurrence(4), disease-free survival(5), malignancy(6), molecular subtypes(7), Ki-67 expression level(8), lymph node metastasis(9–11), response to neoadjuvant chemotherapy(12–14), etc. Our group(11) also developed a radiomics pipeline to predict sentinel lymph node (SLN) metastasis in breast cancer using image features extracted from the primary tumor. The SLN status, which is currently determined by invasive SLN biopsy, is a valuable prognostic factor for breast cancer patients. Our previously published radiomics pipeline achieved a promising prediction performance with a high negative predictive value (NPV), providing non-invasive imaging markers to evaluate SLN status. The high NPV indicates that the prediction model could greatly benefit breast cancer patients, especially those with negative SLN, eliminating unnecessary invasive SLN biopsy and avoiding overtreatment from axillary dissection and its associated serious complications(15).

Although the majority of breast cancer radiomics studies have focused on intratumoral features(4–10, 12), there is evidence that peritumoral features also provide complementary information(13, 14, 16–28). Recent development in breast cancer research has demonstrated that various crucial outcomes are indicated by changes in the tissue surrounding the tumors, such as angiogenic factors(16), peritumoral lymphatic and blood vessel invasion(17, 18), lymphangiogenesis(19), peritumoral lymphocytic infiltration(20), stromal response(21)

and peritumoral edema(22–24). These reports suggest that the peritumoral region may contain valuable information about the tumor. Indeed, some recent publications have taken advantage of peritumoral features. Our previous study(11) included peritumoral features extracted from a dilated region with thickness of ~4mm surrounding the breast lesion on dynamic contrast-enhanced MRI (DCE-MRI) to improve the prediction performance on SLN status in breast cancer. Braman et al (13, 14) reported that a combination of intratumoral and peritumoral radiomic features from pretreatment DCE-MRI could more accurately predict pathological complete response to neoadjuvant chemotherapy for breast cancer patients; the peritumoral regions in their studies were defined by either a varying 2.5- to 5-mm radius or 5 annular rings of 3mm each surrounding the tumor. Peritumoral features have also been used in radiomics studies investigating lung cancer, liver cancer, etc (25–28). These studies suggest that peritumoral features could provide valuable information in radiomic analysis.

However, the optimal peritumoral region size has not yet been systematically investigated in the current literature. The purpose of this study is to further investigate the usefulness of peritumoral features by exploring the effect of the peritumoral region sizes on the prediction performance in the radiomic analysis for predicting SLN status in breast cancer.

Materials and Methods

This retrospective study was approved by our Institutional Review Board.

Dataset

A total of 162 breast cancer patients at our institution were identified, and their DCE-MRI scans and clinicopathological characteristics were collected. The details of the inclusion and exclusion criteria were described in(11), and an additional study was excluded due to incomplete data. Patient characteristics are provided in Table 1.

The DCE-MRI scans were performed with 8-channel breast coils on 1.5T GE Signa HDxt scanners (GE healthcare, Wauwatosa, Wisconsin). Intravenous injection of gadolinium contrast (Magnevist, Schering, Berlin, Germany) was administered at a dose of 0.2ml/kg at a rate of 2 ml/s and followed by a 20-ml saline flush at a rate of 2 ml/s. One pre-contrast (prior to the contrast injection) and four post-contrast phases (at 2, 4, 6 and 8 minutes after contrast administration) were acquired using a VIBRANT sequence in sagittal plane with the following parameters: repetition time (TR)= 4.46~7.80ms; echo time (TE) = 1.54~4.20ms; flip angle=10°; slice thickness = 2mm; matrix size=256X256; pixel size = 0.7 X 0.7 mm^2.

ROI Segmentation and Processing

Regions-of-interest (ROIs) covering the whole tumor were manually drawn slice by slice on the first post-contrast images in sagittal plane using MRIcron (version 4AUGUST2014, open source software; https://www.nitrc.org/projects/mricron) by two expert radiologists independently (R1, with 11 years of experience in breast MRI, and R2, with 10 years' experience). The two radiologists were blinded to the clinicopathologic characteristics and each other's delineation when drawing the ROIs. When there were multiple tumor ROIs in

the breasts, only the largest one was used for analysis. The peritumoral regions were then obtained using MATLAB 2017b by dilating the intratumoral ROIs by 2mm, 4mm, 6mm and 8mm in 3D. The dilation of the ROI was achieved by convoluting the ROIs with a 3D box kernel to achieve the desired size. As the in-plane resolution (0.7mm) is higher than the slice thickness (2mm), the convolution kernel was adjusted to match the voxel size. The regions outside the breasts after dilation were excluded for further analysis. A representative DCE-MRI image and its corresponding ROIs are shown in Figure 1. The radiomic features were extracted from both the intratumoral ROIs and the peritumoral ROIs. The usefulness of peritumoral features were evaluated in our radiomics pipeline by using different peritumoral region sizes (2mm, 4mm, 6mm and 8mm respectively, and also the one among these sizes that generated the peritumoral volume closest to the intratumoral volume for each patient).

Feature Extraction

Radiomic features were extracted from three maps: wash-in maps ((S1-S0)/S0)×100%, wash-out maps ((S1-S4)/S1))×100% and signal enhancement ratio (SER) maps ((S1-S0)/(S4-S0))×100%, where S0, S1, and S4 are the pre-contrast, first post-contrast and fourth (the last) post-contrast images, respectively. These ratio maps reflect the changes in contrast agent concentration and allow direct comparison of the extracted features across patients.

Five categories of features were extracted: (1) shape features (in LIFEx v4.00(29) and MATLAB 2017b), (2) histogram features (in LIFEx), (3) texture features (in LIFEx), (4) Laws features(30) (in MATLAB), and (5) CoLlAGe features(31) (in MATLAB). Shape features were extracted only from the intratumoral ROIs, while features of the other three categories were extracted from both intratumoral ROIs and the peritumoral ROIs with different peritumoral sizes. For each patient, a total of 359 radiomic features were finally extracted in the intratumoral ROI, and 351 radiomic features were extracted in each peritumoral ROI (see Supplementary Table S1 for a detailed list of the extracted features).

Feature Selection and Prediction Model Generation (in training set)

In order to avoid overfitting due to the large amount of extracted features, we randomly separated our dataset two independent subsets: a training set (~67%, 108 patients with 37 positive SLN) and a validation set (~33%, 54 patients with 18 positive SLN). The training set was used for feature selection and prediction model generation.

Before feature selection, data rebalance in the training set was first performed. As significant prediction bias could be caused by class imbalance (samples tend to be classified into the majority group), new samples were synthesized for the minority group using the adaptive synthetic sampling approach for imbalanced learning algorithm(32). The feature selection was then conducted on the rebalanced training set.

For feature selection, a Mann-Whitney U-test was first performed as a backward selection to identify those radiomic features with p-value<0.05 between patients with positive and negative SLN. Next, in order to remove redundant features, each group of highly correlated radiomic features (Spearman $|\rho| \geq 0.95$) was represented by the one with the highest discriminative power, that is, area under the receiver operating characteristic (ROC) curve (AUC) furthest from 0.5 on predicting SLN metastasis. The remaining radiomic

features were then combined with the 7 clinicopathologic characteristics shown in Table 1 as input for least absolute shrinkage selection operator (LASSO) regression. A logistic LASSO model with 3-fold cross-validation was implemented to select the most important predictors, i.e. those features with nonzero coefficients when the minimum cross-validation error plus one standard deviation was reached. In order to avoid overfitting caused by the use of too many features in the prediction model, the maximum number of the selected features were restricted to 10. The selected most important features were used to establish logistic regression models to predict SLN metastasis in breast cancer. The optimal threshold of the ROC prediction analysis was determined by maximizing the Youden index (sensitivity+specificity−1).

As the training dataset was randomly divided into 3 groups in the 3-fold cross-validation LASSO model, this procedure was repeated 100 times with different random seeds. The model that achieved the highest accuracy in the training set was selected as the prediction model for further validation. The corresponding AUC, sensitivity, specificity, NPV and accuracy were calculated.

The above steps in this section were repeated by using the radiomic features extracted from ROIs drawn by R1 and R2, respectively, and also without peritumoral features (peritumoral size = 0mm) and with peritumoral features generated by different peritumoral sizes (2mm, 4mm, 6mm, 8mm respectively, and the one with peritumoral volume closest to the intratumoral volume for each patient). All of the procedures in this section were conducted in MATLAB R2017b.

Prediction Performance Evaluation (in validation set)

The prediction performance of the model generated for each condition was further tested in the independent validation set using the same threshold determined in the training set. The corresponding AUC, sensitivity, specificity, NPV and accuracy were calculated.

Results

Tables 2 and 3 demonstrate the prediction performance in the training and validation sets when incorporating the peritumoral features derived from different peritumoral region sizes (0mm, 2mm, 4mm, 6mm, 8mm, and the one with peritumoral volume closest to the intratumoral volume for each patient) using ROIs drawn by R1 and R2, respectively. The selected features of each model were provided in the Supplementary Tables S2 and S3. When peritumoral features were input for feature selection and model generation, the final selected features of the prediction models all included several peritumoral features.

Table 4 shows the changes in prediction performance, particularly the AUC, NPV and accuracy, in the independent validation set after incorporating the peritumoral features with different peritumoral sizes using R1's and R2's ROIs. As shown in the tables, the prediction performance could be improved when combining peritumoral features into the radiomic analysis (0mm vs other sizes), showing the usefulness of peritumoral features in predicting SLN status in breast cancer. For R1's ROIs, using 6mm as the thickness of the peritumoral regions could achieve the highest accuracy in the validation set. For R2's ROIs, both 4mm

and 8mm yielded higher accuracy compared to other sizes. This suggests the prediction performance of the radiomics models can be further improved by optimizing the peritumoral region sizes. The level of improvement was affected by the choice of the peritumoral size and also the ROI drawing. It also needs to be noted that the optimal peritumoral sizes mentioned above are likely to be specific to this particular application.

An *ad hoc* analysis was also performed to compare the prediction performance between different molecular subtypes and histological grades in the validation set. As our dataset was not sufficient to draw any conclusion and it is out of the scope of this study, we included these interesting results in the Supplementary data section (Supplementary Tables S4 and S5).

Discussion

This is the first work attempting to systematically investigate the prediction performance improvement from peritumoral features in radiomic analysis by exploring the effect of peritumoral region sizes in breast cancer. By performing radiomic analysis for predicting SLN status in breast cancer, we demonstrate that the prediction performance of the radiomic model can be improved when incorporating peritumoral features. This finding confirms the observation in some previous radiomics studies that peritumoral region provides additional information about the tumor (13, 14, 25–28).

In this study, the peritumoral features were generated with peritumoral thicknesses of 2mm, 4mm, 6mm and 8mm, and they were inputted respectively to the radiomics pipeline together with the intratumoral features and clinical characteristics. Prediction performance improvement was observed when using the two radiologists' ROIs with different peritumoral sizes. Our results not only demonstrate the usefulness of peritumoral features in radiomics, but also indicates the choice of the peritumoral size affects the prediction results of the radiomics pipeline. Instead of using arbitrary or uncertain peritumoral region sizes (as most of the current radiomics studies used when including peritumoral features), we suggest the optimal peritumoral thickness should be explored with systematic comparison, which could further improve the prediction model and optimize its performance.

The level of improvement in the prediction performance was affected by not only the choice of the peritumoral size but also the ROI delineation. In this study, the peritumoral regions were determined by dilating the manually annotated tumor ROIs by two expert radiologists, and the prediction performance and the level of improvement brought by peritumoral features were different for these two sets of ROIs. As this study focused on investigating the effect of peritumoral region sizes on the prediction performance of the radiomic models, the inter-reader reliability of the ROIs and the radiomics features was beyond the scope of this study and not practical due to the large number of features included in this analysis. In this study, separate radiomic models were trained for each radiologist. As a result, as long as their own ROI drawing is consistent, the model should be able to learn such drawing habits. In fact, the variations in the ROIs drawn by different radiologists are inevitable as they have their own drawing habits. Although deep learning-based automated breast lesion segmentation has been developed(33), such automated segmentation method

was found to mimic the drawing behavior of the radiologist whose ROIs were used to train the segmentation network. Therefore, when establishing an “end-to-end” radiomics pipeline, the optimization of prediction performance using peritumoral features actually depends on the ROI drawing, which should be taken into consideration for further radiomics studies.

This study has some limitations. The effect of the peritumoral sizes on radiomic analysis depends on different clinical questions and various factors, including the image modalities, scanners, sequence protocols and image resolutions. Our study only focuses on the usefulness of peritumoral features in the specific radiomic application of predicting SLN status in breast cancer patients using the routine DCE-MRI data collected in our institute. Future work includes the combination of different MRI contrasts and the investigation of the impact of tumor subtypes using a larger dataset, ideally with an external validation. More explorations are needed to validate the effect of peritumoral sizes on radiomic analysis in other studies, and the optimal peritumoral size should be determined based on the specific applications.

In conclusion, this study further demonstrates the usefulness of peritumoral features in radiomic analysis in breast cancer, suggesting that peritumoral features contain important information of tumor characteristics and should be included in future radiomics studies. Furthermore, this study is also the first attempt to systematically explore the effect of peritumoral sizes in radiomic analysis in breast cancer. As the choice of the peritumoral size would affect the final prediction performance of the radiomic model, this study suggests that peritumoral features should also be optimized in future radiomics studies.

Supplementary Material

Refer to Web version on PubMed Central for supplementary material.

Abbreviation key:

AUC	area under the receiver operating characteristic curve
DCE-MRI	dynamic contrast-enhanced MRI
LASSO	least absolute shrinkage selection operator
NPV	negative predictive value
ROC	receiver operating characteristic
ROI	region-of-interest
SER	signal enhancement ratio
SLN	sentinel lymph node
TE	echo time
TR	repetition time

References

1. Lambin P, Rios-Velazquez E, Leijenaar R, et al. Radiomics: extracting more information from medical images using advanced feature analysis. European journal of cancer. 2012; 48(4):441–6. [PubMed: 22257792]
2. Gillies RJ, Kinahan PE, Hricak H. Radiomics: images are more than pictures, they are data. Radiology. 2015; 278(2):563–77. [PubMed: 26579733]
3. Lambin P, Leijenaar RT, Deist TM, et al. Radiomics: the bridge between medical imaging and personalized medicine. Nature reviews Clinical oncology. 2017.
4. Li H, Zhu Y, Burnside ES, et al. MR imaging radiomics signatures for predicting the risk of breast cancer recurrence as given by research versions of MammaPrint, Oncotype DX, and PAM50 gene assays. Radiology. 2016; 281(2):382–91. [PubMed: 27144536]
5. Park H, Lim Y, Ko ES, et al. Radiomics signature on magnetic resonance imaging: association with disease-free survival in patients with invasive breast cancer. Clinical Cancer Research. 2018; 24(19):4705–14. [PubMed: 29914892]
6. Bickelhaupt S, Paech D, Kickingereder P, et al. Prediction of malignancy by a radiomic signature from contrast agent-free diffusion MRI in suspicious breast lesions found on screening mammography. Journal of Magnetic Resonance Imaging. 2017; 46(2):604–16. [PubMed: 28152264]
7. Li H, Zhu Y, Burnside ES, et al. Quantitative MRI radiomics in the prediction of molecular classifications of breast cancer subtypes in the TCGA/TCIA data set. NPJ breast cancer. 2016; 2:16012. [PubMed: 27853751]
8. Liang C, Cheng Z, Huang Y, et al. An MRI-based radiomics classifier for preoperative prediction of Ki-67 status in breast cancer. Academic radiology. 2018; 25(9):1111–7. [PubMed: 29428211]
9. Han L, Zhu Y, Liu Z, et al. Radiomic nomogram for prediction of axillary lymph node metastasis in breast cancer. European radiology. 2019:1–10.
10. Dong Y, Feng Q, Yang W, et al. Preoperative prediction of sentinel lymph node metastasis in breast cancer based on radiomics of T2-weighted fat-suppression and diffusion-weighted MRI. European Radiology. 2017:1–10.
11. Liu C, Ding J, Spuhler K, et al. Preoperative prediction of sentinel lymph node metastasis in breast cancer by radiomic signatures from dynamic contrast-enhanced MRI. Journal of Magnetic Resonance Imaging. 2019; 49(1):131–40. [PubMed: 30171822]
12. Wu J, Gong G, Cui Y, Li R. Intratumor partitioning and texture analysis of dynamic contrast-enhanced (DCE)-MRI identifies relevant tumor subregions to predict pathological response of breast cancer to neoadjuvant chemotherapy. Journal of Magnetic Resonance Imaging. 2016; 44(5):1107–15. [PubMed: 27080586]
13. Braman NM, Etesami M, Prasanna P, et al. Intratumoral and peritumoral radiomics for the pretreatment prediction of pathological complete response to neoadjuvant chemotherapy based on breast DCE-MRI. Breast Cancer Research. 2017; 19(1):57. [PubMed: 28521821]
14. Braman N, Prasanna P, Whitney J, et al. Association of peritumoral radiomics with tumor biology and pathologic response to preoperative targeted therapy for HER2 (ERBB2)–positive breast cancer. JAMA network open. 2019; 2(4):e192561–e. [PubMed: 31002322]
15. Recht A, Houlihan MJ. Axillary lymph nodes and breast cancer. A review. Cancer. 1995; 76(9):1491–512. [PubMed: 8635050]
16. Locopo N, Fanelli M, Gasparini G. Clinical significance of angiogenic factors in breast cancer. Prognostic variables in node-negative and node-positive breast cancer: Springer; 1998; 249–63.
17. Lee A, DeLellis RA, Silverman ML, Heatley GJ, Wolfe HJ. Prognostic significance of peritumoral lymphatic and blood vessel invasion in node-negative carcinoma of the breast. Journal of Clinical Oncology. 1990; 8(9):1457–65. [PubMed: 2202788]
18. Gasparini G, Weidner N, Bevilacqua P, et al. Tumor microvessel density, p53 expression, tumor size, and peritumoral lymphatic vessel invasion are relevant prognostic markers in node-negative breast carcinoma. Journal of Clinical Oncology. 1994; 12(3):454–66. [PubMed: 7509851]
19. Christiansen A, Detmar M. Lymphangiogenesis and cancer. Genes & cancer. 2011; 2(12):1146–58. [PubMed: 22866206]

20. Ocaña A, Diez-González L, Adrover E, Fernández-Aramburo A, Pandiella A, Amir E. Tumor-infiltrating lymphocytes in breast cancer: ready for prime time? Journal of Clinical Oncology. 2015; 33(11):1298–9. [PubMed: 25753437]
21. Conklin MW, Keely PJ. Why the stroma matters in breast cancer: insights into breast cancer patient outcomes through the examination of stromal biomarkers. Cell adhesion & migration. 2012; 6(3):249–60. [PubMed: 22568982]
22. Schoenegger K, Oberndorfer S, Wuschitz B, et al. Peritumoral edema on MRI at initial diagnosis: an independent prognostic factor for glioblastoma? European journal of neurology. 2009; 16(7):874–8. [PubMed: 19473360]
23. Uematsu T. Focal breast edema associated with malignancy on T2-weighted images of breast MRI: peritumoral edema, prepectoral edema, and subcutaneous edema. Breast Cancer. 2015; 22(1):66–70. [PubMed: 25336185]
24. Bae MS, Shin SU, Ryu HS, et al. Pretreatment MR imaging features of triple-negative breast cancer: association with response to neoadjuvant chemotherapy and recurrence-free survival. Radiology. 2016; 281(2):392–400. [PubMed: 27195438]
25. Patil PD, Bera K, Vaidya P, et al. Correlation of radiomic features with PD-L1 expression in early stage non-small cell lung cancer (ES-NSCLC) to predict recurrence and overall survival (OS). American Society of Clinical Oncology; 2018.
26. Beig N, Khorrami M, Alilou M, et al. Perinodular and intranodular radiomic features on lung CT images distinguish adenocarcinomas from granulomas. Radiology. 2018:180910.
27. Dou TH, Coroller TP, van Griethuysen JJ, Mak RH, Aerts HJ. Peritumoral radiomics features predict distant metastasis in locally advanced NSCLC. PloS one. 2018; 13(11):e0206108. [PubMed: 30388114]
28. Hu H-T, Shen S-L, Wang Z, et al. Peritumoral tissue on preoperative imaging reveals microvascular invasion in hepatocellular carcinoma: a systematic review and meta-analysis. Abdominal Radiology. 2018; 43(12):3324–30. [PubMed: 29845312]
29. Nioche C, Orlhac F, Boughdad S, et al. A freeware for tumor heterogeneity characterization in PET, SPECT, CT, MRI and US to accelerate advances in radiomics. Journal of Nuclear Medicine. 2017; 58(supplement 1):1316-.
30. Laws KI. Textured image segmentation. University of Southern California Los Angeles Image Processing INST; 1980.
31. Prasanna P, Tiwari P, Madabhushi A. Co-occurrence of local anisotropic gradient orientations (CoLlAGe): a new radiomics descriptor. Scientific reports. 2016; 6:37241. [PubMed: 27872484]
32. He H, Bai Y, Garcia EA, Li S. ADASYN: Adaptive synthetic sampling approach for imbalanced learning. 2008 International Joint Conference on Neural Networks (IJCNN 2008): IEEE; 2008; 1322–8.
33. Spuhler KD, Ding J, Liu C, et al. Task-based assessment of a convolutional neural network for segmenting breast lesions for radiomic analysis. Magnetic resonance in medicine. 2019; 82(2):786–95. [PubMed: 30957936]

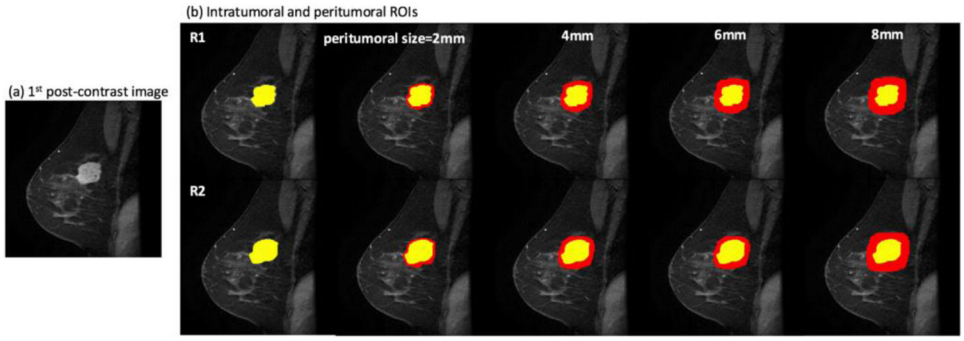

Figure 1.

A representative slice of the input DCE-MRI images and the corresponding ROIs. (a) the first post-contrast image; (b) the intratumoral ROI (yellow regions) drawn by two radiologists R1 (top) and R2 (bottom) with the peritumoral ROIs (red regions) generated by different peritumoral sizes. This case was invasive ductal carcinoma of grade 2, classified into the luminal B subtype.

Table 1

Clinical and histopathological characteristics.

Group	Patients with negative SLN (n=107)	Patients with positive SLN (n=55)	p-value*
Age (mean±SD)	55.6±12.6	55.1±12.9	0.815
Molecular subtype			
Luminal A	44 (41.1%)	16 (29.1%)	0.425
Luminal B	49 (45.8%)	29 (52.7%)	
HER2 positive	4 (3.7%)	4 (7.3%)	
Triple negative	10 (9.4%)	6 (10.9%)	
Histological type			
Invasive ductal carcinoma	87 (81.3%)	49 (89.1%)	0.252
Invasive lobular carcinoma	16 (15.0%)	6 (10.9%)	
Others	4 (3.7%)	0 (0.0%)	
Histological grade			
I	26 (24.3%)	1 (1.8%)	0.001
II	56 (52.3%)	34 (61.8%)	
III	25 (23.4%)	20 (36.4%)	
LVI status			
Negative	98 (91.6%)	20 (36.4%)	<0.001
Positive	9 (8.4%)	35 (63.6%)	
Tumor location (UIQ† or not)			
No	99(92.5%)	53 (96.4%)	0.336
Yes	8 (7.5%)	2 (3.6%)	
Number of other lesions in the ipsilateral breast			
0	99 (92.5%)	51 (92.7%)	0.863
1	6 (5.6%)	3 (5.5%)	
2	1 (0.9%)	1 (1.8%)	
3	1 (0.9%)	0	

*Two-tailed two-sample t-test with unequal variances was used to compare the age. Other characteristics were tested by chi-square cross-tabulation.

†Tumors in UIQ has been shown to have significantly lower frequency of axillary lymph node metastasis compared to tumors in all other quadrants.

Abbreviations: SLN – sentinel lymph node, SD – standard deviation, HER2 – human epidermal growth factor receptor-2, LVI – lymph-vascular invasion, UIQ – upper inner quadrant.

Table 2.

The prediction performance in the training and validation sets when using different peritumoral sizes based on ROIs drawn by R1.

	Training set					Validation set				
	AUC	**Sens**	**Spec**	**NPV**	**Acc**	**AUC**	**Sens**	**Spec**	**NPV**	**Acc**
0mm	0.921	0.924	0.831	0.922	0.876	0.770	0.667	0.722	0.813	0.704
2mm	0.931	0.859	0.873	0.861	0.866	0.761	0.667	0.778	0.824	0.741
4mm	0.942	0.926	0.845	0.923	0.885	0.841	0.778	0.722	0.867	0.741
6mm	0.919	0.922	0.859	0.924	0.889	0.824	0.667	0.861	0.838	0.796
8mm	0.908	0.985	0.775	0.982	0.876	0.776	0.667	0.722	0.813	0.704
Tumor size	0.917	0.929	0.789	0.918	0.858	0.801	0.667	0.750	0.818	0.722

Abbreviations: AUC – area under the receiver operating characteristic curve, Sens – Sensitivity, Spec – Specificity, NPV – negative predictive value, Acc – Accuracy.

Table 3.

The prediction performance in the training and validation sets when using different peritumoral sizes based on ROIs drawn by R2.

	Training set					Validation set				
	AUC	**Sens**	**Spec**	**NPV**	**Acc**	**AUC**	**Sens**	**Spec**	**NPV**	**Acc**
0mm	0.935	0.912	0.873	0.912	0.892	0.793	0.556	0.861	0.795	0.759
2mm	0.960	0.831	0.972	0.852	0.901	0.792	0.722	0.694	0.833	0.704
4mm	0.934	0.944	0.817	0.935	0.881	0.846	0.778	0.806	0.879	0.796
6mm	0.939	0.841	0.915	0.855	0.879	0.812	0.833	0.694	0.893	0.741
8mm	0.932	0.940	0.859	0.938	0.899	0.827	0.778	0.806	0.879	0.796
Tumor size	0.954	0.944	0.845	0.938	0.894	0.829	0.778	0.694	0.862	0.722

Abbreviations: AUC – area under the receiver operating characteristic curve, Sens – Sensitivity, Spec – Specificity, NPV – negative predictive value, Acc – Accuracy.

Table 4.

The prediction performance changes in the validation set when using different peritumoral sizes based on ROIs drawn by R1 and R2.

Changes	R1			R2		
	AUC	NPV	Acc	AUC	NPV	Acc
2mm	− 0.009	+ 0.011	+ 0.037	− 0.001	+ 0.038	− 0.055
4mm	+ 0.071	+ 0.054	+ 0.037	+ 0.053	+ 0.084	+ 0.037
6mm	+ 0.054	+ 0.025	+ 0.092	+ 0.019	+ 0.098	− 0.018
8mm	+ 0.006	0	0	+ 0.034	+ 0.084	+ 0.037
Tumor size	+ 0.031	+ 0.005	+ 0.018	+ 0.036	+ 0.067	− 0.037

Abbreviations: AUC – area under the receiver operating characteristic curve, NPV – negative predictive value, Acc – Accuracy.